

# Dynamics of Morphological Formation Affected by Processing Parameters in Chemical Bath Deposition

Kun-Dar Li<sup>\*</sup>, Sheng-Jie Hong<sup>\*\*</sup>, Han-Lin Hu<sup>\*\*</sup> and David Ta-Wei Lin<sup>\*\*\*</sup>

**Keywords:** Crystallographic effect, Chemical bath deposition, Modeling, Phase field deposition.

## ABSTRACT

Attracting by the simple processes with wide applications, even for a long time of development the chemical bath deposition method is still one of the most popular techniques utilized in many modern and advanced manufacturing fields. In this study, a numerical model is applied to explore the formation mechanisms of a chemical bath deposition and rebuilt the structural evolution of precipitation films during this process. Regarding to the feasibility of this model, various experimental parameters affecting the structural morphologies are taken into consideration to theoretically reveal their influences in the chemical bath deposition process. One of the major contributions in this study is on the characterization of the anisotropic growth with a three-dimensional anisotropic model in a chemical bath deposition, which is unique to the related studies. The factors, including the deposition rate, the preferred growth orientation and diffusion rate are systematically inspected to form miscellaneous surface profiles. From the numerical results, it shows that the pyramid-like surface morphology could be transferred into a four-fold symmetry mountain-like surface morphology by the preferred growth orientation. These numerical simulations visualize the processes of the nucleation and growth of precipitations during a chemical bath deposition. The theoretical model provides a favorable tool for the technological developments of chemical bath

*Paper Received January, 2022. Revised February, 2022.  
Accepted March, 2022. Author for Correspondence: David T.W. Lin.*

*\* Professor, Department of Materials Science, National University of Tainan, Tainan 70005, Taiwan*

*\*\* Department of Materials Science, National University of Tainan, Tainan 70005, Taiwan*

*\*\*\* Professor, Department of Materials Science, National University of Tainan, Tainan 70005, Taiwan*

## INTRODUCTION

Chemical bath deposition, also known as chemical solution deposition, has been developed for a long time to deposit different types of film materials. With the advantages of low process temperature, low cost, and mass production (Surabhi et al., 2021; Ghobadi et al., 2020; Pourshaban et al., 2016; Min, 2016; Qu et al., 2017), chemical bath deposition is applied widely and plays a crucial role in many fields of modern industries, such as photovoltaic cells, photoelectrochemical cells, multilayer ceramic capacitors, and solid oxide fuel cells (Cao et al., 2021; Zhang et al., 2020; Hodes, 2002; Schneller et al., 2013). By immersing the substrate in a proper precursor solution, various film materials could be produced on substrates through the process of chemical bath deposition. Including the precursor, additive materials, solution concentration, temperature, processing time, and type of substrate, many parameters in the chemical bath deposition process could significantly affect the properties of deposited films (Duan et al., 2020; Arandhara et al., 2020; Chol et al., 2021; Govender et al., 2004; Pauporte, 2014), such as the structural, morphological, crystallographic, electrical and optical features. While the temperature, pH, and concentration of the solution are manipulated, the nucleation and growth processes of film formation can be tailored. Simultaneously, the final properties of films would be altered accordingly. Depending on the processing parameters, in a chemical bath deposition a variety of film morphologies can be obtained, such as the sponges, honeycombs, ribbons, spheres, sheets, cubes and hexagonal platelets of deposited films (Schneller et al., 2013; Roa et al., 2021; Tonagi et al., 2020; Gu et al., 2020; Yahiroet al., 2007; Lipowsky et al., 2008; Lipowsky et al., 2006). The influence of the different morphologies and textures on the performance properties shows the importance of the precise control over film growth. To possess the capability of managing the growth rates, structures, and properties

of the deposited films, it is essential to comprehend the operating process of chemical bath deposition and the mechanisms of film formation thoroughly. In spite of the simplicity in the experimental process, understanding the mechanisms involved in the deposition and gaining the ability to widen the range of deposits are not so simple. Usually, these reactions are governed by the thermodynamics and kinetics of chemical deposition as the materials are transformed into the desired crystalline thin films with proper phase, microstructure, texture, and pattern.

In the past decades, a chemical bath deposition process was analyzed by a chemical engineering method (Kostoglou et al., 2000) to construct model equations, based on a population balance formulation. Including the nucleation and surface reaction, a possible sequence of formation mechanisms was suggested for the temporal variations of reactant concentrations with the solid phase, and a comprehensive model of chemical bath deposition was solved numerically. Since this type of models was focusing on the kinetics of the process, some factors affecting the film morphology was not take into consideration. Furthermore, in the initial stage of the film formation the shape and spatial distribution of the nuclei also have a dramatical influence on the quality and thickness of final films. A simple phenomenological model based on a direct Monte Carlo simulation (Kostoglou et al., 2003) was implemented to simulate the initial stages of film growth behavior for the film deposition. Recently, the developments of kinetic roughening theory (Gupta and Mohanty, 2016) for the roughness evolution of film growth have attracted extensive attention. As well acknowledged, the roughness evolution of a surface is associated with a consequence of simultaneous atomic scale processes, such as direct addition of atoms on the growing surface from the surrounding, removal of atoms from the surface and motion of atoms along the surface or diffusive mass transport due to an existing or increasing chemical potential gradient. The establishment of surface evolution processes could provide the detailed insight into the fundamental growth dynamics and acquire the ability of controlling the film roughness. Nowadays, for simulating the mesoscale processes the other powerful tool known as the phase-field technique is more appropriate and popular (Moelans et al., 2008). The phase-field approach has been used in a wide range of applications from the solidification, solid-state phase transformations, grain growth, dislocation dynamics to solid-state sintering (Henry and Levine, 2004; Jing et al., 2005; Wang, 2006). Also, with the computing power increasing at an extreme rate, it stimulates the rapid development of computer simulation technology in the last decade.

In order to evaluate the formation mechanisms and reconstruct the surface evolution of thin films in the process of chemical bath deposition, in this study a numerical method based on the phase-field model is

applied to establish theoretical simulations for chemical bath deposition. Furthermore, various parameters affecting the structural morphologies, such as the deposition rate, the preferred growth orientation and diffusion rate, are also examined to demonstrate the influences on the process of films development. In this study, an anisotropic model is implemented to characterize the behaviors of the crystallographic-direction related growth during a chemical bath deposition in three dimensions. Depending on the different processing parameters, miscellaneous surface profiles with featured morphologies are reconstructed. In the current research, much attention is also given to the quantitative aspects of the simulations, such as the parameter assessment and surface features. With the systemic studies, this paper is expected to provide comprehensive information for chemical bath deposition process by phase-field modeling. The basic concepts are explained and illustrated with the numerical simulations to show the possible applications of the chemical bath deposition for advanced manufacturing.

## NUMERICAL MODEL

To construct a numerical model for a chemical bath deposition, the mechanisms of the deposition process needs to be dealt with. According to previous literatures (Hodes, 2002), the primary reaction in a chemical bath deposition could be rationally concentrated on the precipitation process. Including a homogeneous nucleation in solution or heterogeneous nucleation on a substrate, following with growth process, a concise mechanism of chemical deposition process can be simply established. Regarding to the nucleation and growth process of a precipitate, various physical processes with thermodynamic and kinetic factors must be considered. More detailed descriptions of precipitation phenomena for a chemical deposition, such as the homogeneous/heterogeneous nucleation, atomic/ionic adsorption, surface diffusion, etc., can be referred to Hodes (2002). Complying with the methodology of the phase field approach, the physical phenomena involved in the microstructural evolution of chemical deposition are demonstrated. In this numerical model, the phases of the adatoms and substrate are firstly defined by two field variables,  $c_a$  and  $c_s$ , which represent the concentrations of the adatoms and substrate. Then, the thermodynamic state of this dual-variables system indicated by the free energy  $G$  could be formulated as (Li and Dong, 2017; Chen and Yang, 1994; Warren et al., 2003):

$$G = \int \left[ (1 - w_s) \left\{ g(c_a) + \frac{\epsilon_a^2}{2} |\nabla c_a|^2 \right\} + w_s \left\{ g(c_s) + \frac{\epsilon_a^2}{2} |\nabla c_a|^2 \right\} + (1 - w_a) \frac{\epsilon_s^2}{2} |\nabla c_s|^2 \right] dV \quad (1)$$

where  $g(c_a)$  and  $g(c_s)$  are the local free energies for the adatoms phase and substrate phase, respectively.  $w_s$  and  $w_a$  are monotonically increasing functions of the

variables  $c_s$  and  $c_a$  to denote the contributions of each phase. One of the simplest expressions is  $w_s = c_s$  and  $w_a = c_a$  (Warren et al., 2003). To cope with the local free energies of  $g(c_a)$  and  $g(c_s)$ , a regular solution model of atom-vacancy complex system is employed (Asp and Agren, 2006), e.g.  $g(c_a) = g_a c_a + g_v(1 - c_a) + Nk_B T [c_a \ln c_a + (1 - c_a) \ln(1 - c_a)] + N\Omega c_a(1 - c_a)$ , where  $g_a$  is the molar free energy of adatoms per unit volume and  $g_v$  is the molar free energy of vacancy per unit volume,  $N$  is the number of atoms per unit volume,  $k_B$  is the Boltzmann's constant,  $T$  is the absolute temperature, and  $\Omega$  is the parameter of interatomic bond energy.

The coefficients of  $\varepsilon_{a-l}$ ,  $\varepsilon_{a-s}$  and  $\varepsilon_{s-l}$  in the gradient concentration terms of Eq. (1) represent the interfacial energies between different phases, such as the adatoms and solution, the adatoms and substrate, and the substrate and solution. During a chemical deposition, crystalline precipitates are usually formed on the substrate. Therefore, the anisotropic interfacial energies should be taken into consideration. Dealing with an anisotropic phase-field model, a unit normal vector ( $\mathbf{n}$ ) of the interface is defined by  $\nabla c_i / |\nabla c_i|$ , where  $c_i$  is the field variable, and the subscript  $i$  can be  $a$  or  $s$  to indicate the adatoms phase or substrate phase. Then, the physical quantities, which are functions of the crystallographic orientation, can be described by the polar angle ( $\Theta = \cos^{-1} \left( \frac{c_{iz}}{|\nabla c_i|} \right)$ ) and the azimuthal angle ( $\Phi = \tan^{-1} \left( \frac{c_{iy}}{c_{ix}} \right)$ ), where  $c_{ix}$ ,  $c_{iy}$  and  $c_{iz}$  are the partial differentiations of the field variable with respect to the axes of  $\mathbf{x}$ ,  $\mathbf{y}$ , and  $\mathbf{z}$ , respectively. The anisotropic interfacial energies in Eq. (1) are further expressed as  $\varepsilon_{a-l}(\Theta, \Phi)$ ,  $\varepsilon_{a-s}(\Theta, \Phi)$  and  $\varepsilon_{s-l}(\Theta, \Phi)$ . As the adatoms and the substrate phases are regarded as an identical crystalline structure, the anisotropy of the interfacial energies would be the same, e.g.  $\varepsilon_{a-l}(\Theta, \Phi) = A(\Theta, \Phi) \cdot \varepsilon_{a-l}$ ,  $\varepsilon_{a-s}(\Theta, \Phi) = A(\Theta, \Phi) \cdot \varepsilon_{a-s}$  and  $\varepsilon_{s-l}(\Theta, \Phi) = A(\Theta, \Phi) \cdot \varepsilon_{s-l}$ , where  $A(\Theta, \Phi)$  is the anisotropy parameter. For a cubic crystal system, the anisotropy parameter  $A(\Theta, \Phi)$  of the interfacial energy could be written as (Kim, 2007):

$$A(\Theta, \Phi) = (1 - 3\lambda) \left[ 1 + \frac{4\lambda}{1-3\lambda} (\sin^4 \Theta \cdot (\sin^4 \Phi + \cos^4 \Phi) + \cos^4 \Theta) \right] \quad (2)$$

where  $\lambda$  is the strength of anisotropy.

The adatoms diffusion is one of the most significant effects in the morphological evolution. The driving force for the adatoms diffusion is attributed to the gradient of the chemical potentials. The chemical potential of adatoms is obtained by differentiating the free energy  $G$  of the system with the field variable of  $c_a$ . While the gradient of the chemical potential is established, the movement of adatoms along the down-gradient would be implemented until the equilibrium is reached again. Thus, the diffusion flux  $\mathbf{J}$  of adatoms could be given as a quantity proportional to the

gradient of the chemical potential. This proportional constant is known as the mobility of adatoms. Furthermore, a time dependence of adatom concentration could be acquired as the conservation equation with source term is obeyed, such as  $N \frac{\partial c_a}{\partial t} = -\nabla \cdot \mathbf{J} + S$  where  $S$  represents the depositing adatoms. Combining with all the physical conditions, an anisotropic diffusion equation describing the spatially temporal function of adatoms during a chemical deposition is derived as,

$$\begin{aligned} \frac{\partial c_a}{\partial t} = & \frac{1}{N^2} \nabla \cdot \left( M_a(\Theta, \Phi) \nabla \left( (1 - c_s) \frac{\partial g(c_a)}{\partial c_a} - \right. \right. \\ & \left. \left. \frac{\varepsilon_{s-l}^2}{2} |\nabla c_s|^2 - ((1 - c_s) \cdot \varepsilon_{a-l}^2 + \right. \right. \\ & \left. \left. c_s \cdot \varepsilon_{a-s}^2) \cdot \left( \nabla \cdot (A(\Theta, \Phi)^2 \nabla c_a) + \right. \right. \right. \\ & \left. \left. \frac{\partial_x}{\partial x} \left( |\nabla c_a|^2 A(\Theta, \Phi) \frac{\partial c_{ax}}{\partial c_a} A(\Theta, \Phi) \right) + \right. \right. \\ & \left. \left. \frac{\partial_y}{\partial y} \left( |\nabla c_a|^2 A(\Theta, \Phi) \frac{\partial c_{ay}}{\partial c_a} A(\Theta, \Phi) \right) + \right. \right. \\ & \left. \left. \left. \frac{\partial_z}{\partial z} \left( |\nabla c_a|^2 A(\Theta, \Phi) \frac{\partial c_{az}}{\partial c_a} A(\Theta, \Phi) \right) \right) \right) \right) + \frac{S}{N} \quad (3) \end{aligned}$$

where  $M_a(\Theta, \Phi)$  is the anisotropic mobility of adatoms. The anisotropic mobility could also be described as  $M_a(\Theta, \Phi) = M_{a_0} \cdot (A(\Theta, \Phi))^{-2}$  (McFadden et al., 1993), where  $M_{a_0}$  is the average mobility of adatoms. Regarding to the chemical deposition behavior in the source term,  $S/N$  could be further formulated as,

$$\frac{S}{N} = S_a(1 - c_s) |\nabla c_a|^2 + S_s(1 - c_a) |\nabla c_s|^2 \quad (4)$$

where  $S_a$  is the deposition flux of adatoms on the surface of precipitates and  $S_s$  is the deposition flux of adatoms on the surface of uncovered substrate. In addition, owing to the crystallographic symmetry, the deposition flux of adatoms affected by the chemical reactions could be functions of the crystallographic orientation. Equation 4 has dealt with the prominent feature of formation mechanisms during a chemical bath deposition process. If further factors are considered or the reaction is changed, such as the substrate, film materials, precursor or solution concentration, the deposition flux of adatoms on the surface of precipitates ( $S_a$ ) and the deposition flux of adatoms on the surface of uncovered substrate ( $S_s$ ) in Eq. 4 could be modified accordingly to describe the related mechanisms properly in a chemical bath deposition. Again, assuming the identical anisotropy of chemical depositions on the precipitates and substrate, the deposition flux of adatoms is written as:

$$S_i(\Theta, \Phi) = S_i^0 \cdot [I(\Theta, \Phi)]^2 \quad (5)$$

where  $S_i^0$  is the average chemical deposition rate, the subscript  $i$  is either  $a$  or  $s$ , and  $I(\Theta, \Phi)$  presents the anisotropic chemical deposition along the specific crystallographic orientation. While the chemical

deposition occurs along the preferred crystallographic orientation, different mathematical formula associated with the crystallographic orientation should be taken into consideration. Here, two specific growth directions are inspected, such as <100> and <111>. The equations for <100> and <111> crystallographic directions could be expressed as (Younsi and Cartalade, 2016; Dantzig et al., 2013; Podmaniczky et al., 2014):

$$I_{<100>}(\Theta, \Phi) = (1 - 3\eta) \left[ 1 + \frac{4\eta}{1-3\eta} (\sin^4 \Theta \cdot (\sin^4 \Phi + \cos^4 \Phi) + \cos^4 \Theta) \right] \quad (6)$$

and,

$$I_{<111>}(\Theta, \Phi) = [1 + 66\eta \cdot \sin^4 \Theta \cos^2 \Theta \sin^2 \Phi \cos^2 \Phi] \quad (7)$$

where  $I_{<100>}(\Theta, \Phi)$  and  $I_{<111>}(\Theta, \Phi)$  represent the chemical deposition rates along the crystallographic orientations of <100> and <111>, respectively.  $\eta$  is the strength of anisotropy of the chemical deposition rate, affected by the deposition conditions such as the type or concentration of the solution, temperature, etc. Other types of the preferred deposition orientation can also be simulated as an appropriate form of  $I(\Theta, \Phi)$  is applied. If an isotropic chemical deposition condition is considered,  $I(\Theta, \Phi)$  would be equal to 1.

To perform the numerical simulations, a length-scale  $l_0$  and a time-scale  $\tau$  are introduced to simplify the calculations, such as  $l_0 = \varepsilon_0 \cdot (Nk_B T)^{-1/2}$  and  $\tau = \frac{1}{M_{a_0}} \left( \frac{\varepsilon_0}{k_B T} \right)^2$  where  $\varepsilon_0$  is a reference interfacial energy. Accordingly, a dimensionless diffusion equation is derived by normalizing the spatial coordinates and the time of Eq. (3) with  $l_0$  and  $\tau$ ,

$$\begin{aligned} \frac{\partial c_a}{\partial t^*} = \nabla^* \cdot M_a^*(\Theta, \Phi) \nabla^* (1 - c_a) \frac{\partial g^*(c_a)}{\partial c_a} + \\ \nabla^* \cdot M_a^*(\Theta, \Phi) \nabla^* \varepsilon_{s-l}^{*2} \nabla^{*2} c_s - \nabla^* \cdot M_a^*(\Theta, \Phi) \nabla^* \left( (1 - c_s) \cdot \varepsilon_{a-l}^{*2} + c_s \cdot \varepsilon_{a-s}^{*2} \right) \cdot \left( \nabla^* \cdot (A(\Theta, \Phi)^2 \nabla^* c_a) + \right. \\ \left. \partial_{x^*} \left( |\nabla^* c_a|^2 A(\Theta, \Phi) \partial_{c_{a,x^*}} A(\Theta, \Phi) \right) + \right. \\ \left. \partial_{y^*} \left( |\nabla^* c_a|^2 A(\Theta, \Phi) \partial_{c_{a,y^*}} A(\Theta, \Phi) \right) + \right. \\ \left. \partial_{z^*} \left( |\nabla^* c_a|^2 A(\Theta, \Phi) \partial_{c_{a,z^*}} A(\Theta, \Phi) \right) \right) \right) + \\ S_a^* I(\Theta, \Phi)^2 (1 - c_s) |\nabla^* c_a|^2 + S_s^* I(\Theta, \Phi)^2 (1 - c_a) |\nabla^* c_s|^2 \quad (8) \end{aligned}$$

where  $t^*$  is the normalized time,  $x^* = x/l_0$ ,  $y^* = y/l_0$ ,  $z^* = z/l_0$ ,  $\nabla^* = l_0 \nabla$ ,  $M_a^*(\Theta, \Phi) = M_a(\Theta, \Phi)/M_{a_0}$ ,  $\varepsilon_{a-l}^* = \varepsilon_{a-l}/\varepsilon_0$ ,  $\varepsilon_{s-l}^* = \varepsilon_{s-l}/\varepsilon_0$ ,  $\varepsilon_{a-s}^* = \varepsilon_{a-s}/\varepsilon_0$ ,  $S_a^* = \frac{\tau}{l_0^2} S_a^0$  and  $S_s^* = \frac{\tau}{l_0^2} S_s^0$ .

By solving the diffusion equation of Eq. (8), the nucleation and growth process of precipitates in a chemical deposition could be characterized. In this study, the microstructural formation and evolution of crystalline precipitates during processing are reconstructed by the numerical simulations with the finite volume method (Vinokur, 1989). Additionally, in order to investigate the influences of manufacturing parameters on the surface structures, a series of numerical simulations are implemented with various deposition rate, strength of anisotropy and preferred growth orientation. In the numerical model, a three-dimensional mesh with size of  $60 \times 60 \times 60$  is employed, and the grid spacing is 0.5. For the simulation calculations, the time step is 0.5. To present a periodic geometry (Versteeg and Malalasekera, 1995), periodical boundary conditions are introduced in  $x$  and  $y$  axes with zero flux at  $z=0$  and  $z=L_z$ , where  $L_z$  is the size of the mesh in  $z$  direction. Regarding to the deposition substrate, a flat surface is assigned on the bottom of the numerical model. The simulation parameters associated with the chemical deposition process are subject to the literatures, such as  $\varepsilon_0^2 = 8 \times 10^{-19} \text{J}$  (Suo and Lu, 2000),  $\Omega = 1.8 \times 10^{-20} \text{J}$  (Porter et al., 2009),  $N = 1 \times 10^{19} \text{m}^{-2}$  (Yu and Lu, 2005),  $\lambda = 0.06$ , and  $T = 348 \text{K}$  (Mo et al., 1991) for simulation calculations. A series of preliminary calculations are taken for all the numerical parameters to evaluate their applicability under a specific condition of thin film growth. The length scale ( $l_0$ ) is then calculated as  $\sim 4.25 \text{nm}$ . Other essential parameters involving in the nucleation and growth process of precipitates are also altered to reflect various deposition conditions, such as a deposition rate  $S_a^*$ , the anisotropic strength  $\eta$  and the migration coefficient  $M_a^*$ . These parameters used in the numerical simulations are summarized in Table 1 and would be discussed in more detail later.

**Table 1** The calculation parameters used in the numerical simulations

Symbol	Value	Ref.
$\varepsilon_0^2$	$8 \times 10^{-19} \text{J}$	Suo and Lu, 2000
$\Omega$	$1.8 \times 10^{-20} \text{J}$	Porter et al., 2009
$N$	$1 \times 10^{19} \text{m}^{-2}$	Yu and Lu, 2005
$T$	348K	Mo et al., 1991
$\lambda$	0.06	-
$\varepsilon_{a-l}^*$	0.75	-
$\varepsilon_{s-l}^*$	0.5	-
$\varepsilon_{a-s}^*$	0.25	-
$S_s^*$	0.001	-
$S_a^*$	0.1, 0.075, 0.05	-
$\eta$	0.3, 0.1, 0.01	-
$M_a^*$	0.02, 0.01, 0.005	-

To demonstrate the detailed impacts of these factors, the surface characteristics of thickness and surface roughness of precipitates in numerical calculations are analyzed by quantitative measurements. The mean

thickness ( $\bar{D}$ ) of the deposited precipitates is calculated by,

$$\bar{D} = \frac{1}{p^2} \sum_{m=1}^p \sum_{n=1}^p D(m, n) \quad (9)$$

where  $D(m, n)$  is the height of the precipitate at a certain point of the mesh, and  $p$  is the number of the mesh in  $x$  and  $y$  axes. And, the surface roughness of  $R_{RMS}$  is estimated by

$$R_{RMS} = \sqrt{\frac{1}{p^2} \sum_{m=1}^p \sum_{n=1}^p (D(m, n) - \bar{D})^2} \quad (10)$$

## RESULTS AND DISCUSSION

Firstly, a representative result is presented in Fig. 1 for a chemical bath deposition simulated by this model. In this case, a deposition rate  $S_a^*$  of 0.075 with the aforementioned parameters is considered and the film formation and surface morphological evolution are revealed clearly in this figure. During the early stage of deposition, there is no precipitate formed on the substrate surface due to a relatively low concentration of deposited species in this period. After an incubation period, precipitates could be found as shown in Fig. 1(a). While the amounts of precipitates are greatly increased, the isolated precipitates start to connect or coalesce with the others. Then, a labyrinth-like structure is formed on the substrate surface, as demonstrated in Fig. 1(b). By virtue of the accumulation of deposited species for a certain period, a continuous film would be created. A characteristic feature with pyramid-like morphology presents on the surface of the continuous film, as presented in Fig. 1(c). This surface feature is controlled by the anisotropic diffusion and the anisotropic growth of chemical deposition due to the crystallographic symmetry. With the increase of the reaction time, the deposited film become thicker, and the characteristic feature of surface morphology is retained, as shown in Fig. 1(d)-(f). The major differences between these figures in the later stages are the thickness of the film, accompanying with the slight evolution of the pyramid-like surface morphology.

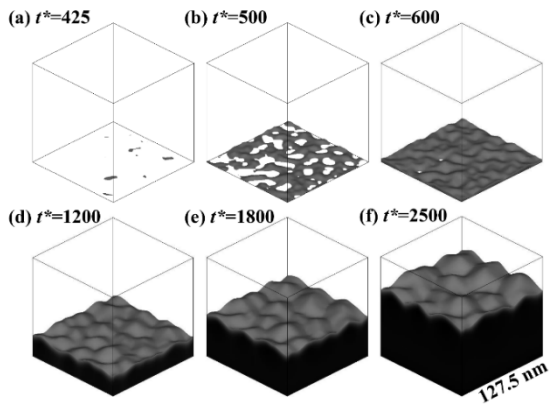
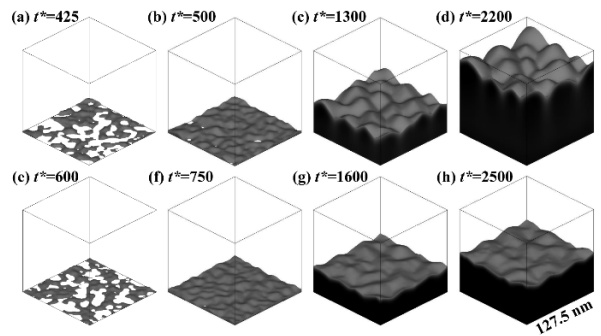


**Fig. 1** A theoretical simulation of chemical deposition process, calculated by Eq. (8):  $t^*$  denotes the

simulation time in arbitrary units

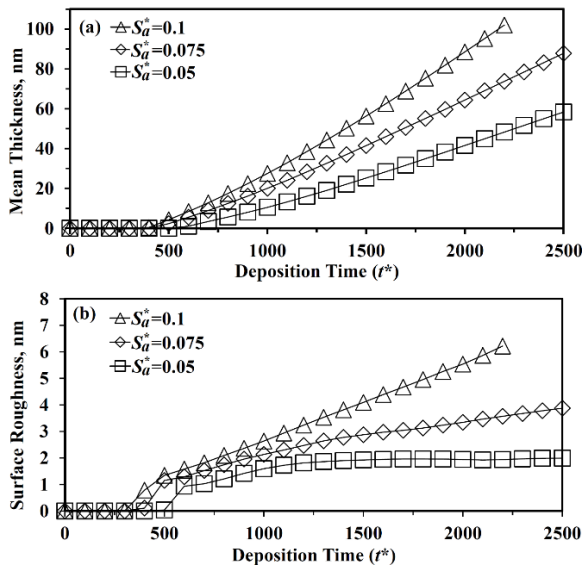
These simulation results based on phase field method have rebuilt the formation and evolution of thin film in a chemical bath deposition, which are consistent well with the experimental observations in Fig. 2 of Ref. Tonagi et al. (2020) and Fig. 3 of Ref. Hone and Dejene (2020). This theoretical model is rational and suitable to investigate the manufacturing processes and the effect of the parameters on the properties of thin films made by chemical bath deposition.

To evaluate the influence of the deposition rate on the thin film formation in the chemical bath deposition, different levels of deposition rate are discussed in the numerical simulations, such as  $S_a^*=0.1$  and 0.05. And, all the other calculation parameters in Fig. 2 are the same as used in Fig. 1, except the deposition rate, to compare the results in the previous case. In Fig. 2(a) to (d), a high deposition rate is demonstrated, while a case with relatively low deposition rate is presented in Fig. 2(e)-(h). In the case of a high deposition rate, it is observed that the particles are formed rapidly in the early stage and the incubation time of deposition reaction is significantly decreased, as shown in Fig. 2(a). While more and more atoms are deposited on the top of substrate, gradually a continuous film is formed as demonstrated in Fig. 2(b). For a longer reaction time, the accumulation of adatoms causes the thickness of film to increase rapidly with strengthened features, as exhibited in Fig. 2(c) and (d). This characteristic surface feature is comparable to Fig. 1(d)-(f). The pyramid-like surface morphologies are mainly induced by the anisotropic surface diffusion. In contrast to the high deposition rate, the case with a low deposition rate of chemical deposition exhibits a moderate growth rate with a similar surface evolution process. The steps of the nucleation, coalescence and the development of film thickness are demonstrated in Fig. 2(e)-(h). In addition to the growth rate, between these conditions one of the major differences is the surface profile. For a low deposition rate, it could be seen that the surface feature is not so obvious with a small surface roughness.



**Fig. 2** Theoretical simulations of chemical deposition process with different deposition rate  $S_a^*$  calculated by Eq. (8): (a)-(d) a high deposition rate of  $S_a^* = 0.1$ , and (e)-(h) a low deposition rate of  $S_a^* = 0.05$

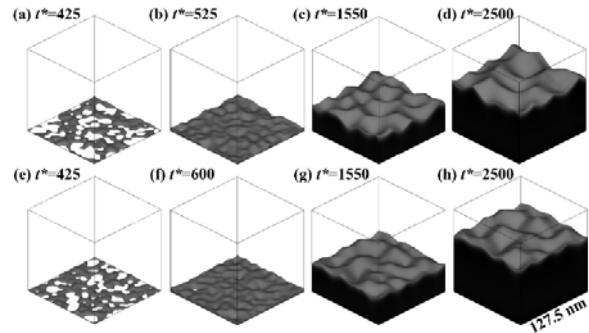
To demonstrate the influence of the deposition rate more clear, the quantitative measurements of the surface thickness and surface roughness for Fig. 1 and 2 are displayed in Fig. 3. From the variation of film thickness with the deposition time in Fig. 3(a), a linear relationship between the thickness and the deposition time could be seen. The slopes of three conditions are 0.0301, 0.0428 and 0.0571 for  $S_a^*=0.05, 0.075$  and  $0.1$ , respectively, which are directly proportional to the parameters of  $S_a^*$  in the numerical simulation. In the roughness measurement of Fig. 3(b), it shows that surface roughness would rise up after the film passes the incubation time. For the case with a low deposition rate, the surface roughness keeps at a low level even at a later stage of deposition. By contrast, while a higher deposition rate is considered, the surface roughness would be increased with the deposition time. In addition, the variation of surface roughness slopes is also proportional to the deposition rate. It might be attribute to the anisotropic growth along the crystallographic directions. Since the certain crystallographic direction possesses a high deposition rate, the surface profile can become roughened with the processing time.



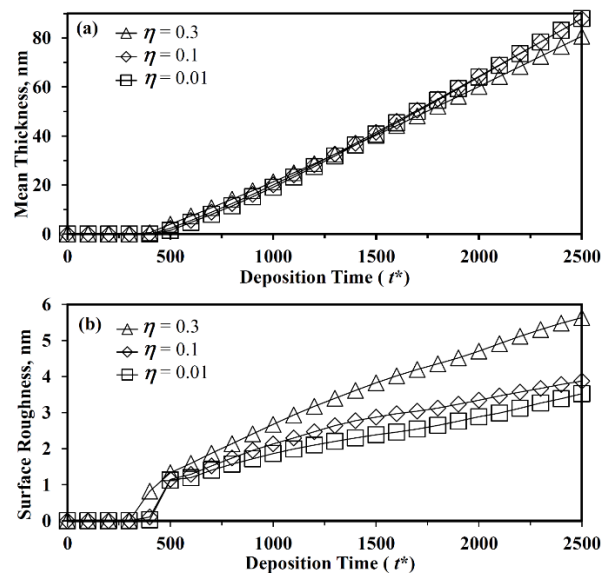
**Fig. 3** The quantitative analyses of the theoretical simulations with different deposition rate  $S_a^*$ : (a) the mean thickness, and (b) the surface roughness

From the previous discussions, the anisotropy of crystalline films plays a significant effect on the thin film formation and surface profile. Thus, different anisotropic strengths are evaluated to reveal its influence on the surface morphology. In Fig. 4(a)-(d) and 4(e)-(h), the values of the anisotropic strength ( $\eta$ ) are 0.3 and 0.1, respectively, to simulate the depositions for the high anisotropy of crystalline materials, while other parameters are the same as used in Fig. 1. From these figures, it could be found that a similar profile evolution process is observed in three levels of anisotropic strength, as shown in Fig. 1 and 4. There is no obvious difference between these surface

morphologies while the anisotropic strength is increased. Only a slight variation on the surface roughness can be sensed. With the increase of the anisotropic strength, surface roughness is increased and the characteristic length of the structures is increased. The quantitative measurements of the film thickness and surface roughness in Fig. 5 reveal the same views of the tiny variations in different conditions of anisotropic strength. In Fig. 5(a), it can be seen that three curves of the film thickness are almost overlapped, and the slopes are around 0.04. Only a little drop of the deposition rate is presented in a high anisotropic strength. The reason is that the films grow more strongly along a certain crystallographic direction, which could reduce the overall growth rate. In Fig. 5(b), it is expressed that a higher surface roughness is produced with the increased anisotropic strength. Corresponding with the surface profile observations in Fig. 4, these quantitative data can demonstrate the surface feature more clearly.

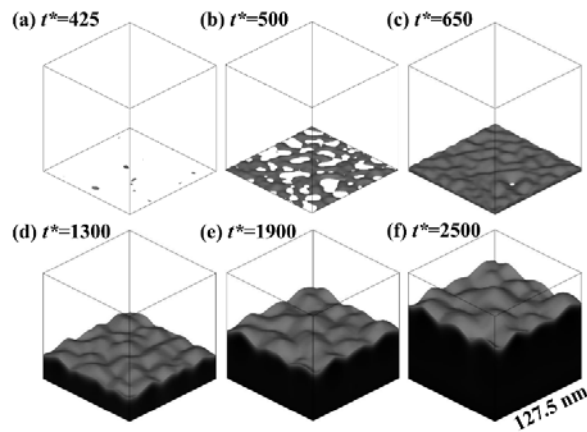


**Fig. 4** Theoretical simulations of chemical deposition process with different anisotropic strength  $\eta$ , calculated by Eq. (8): (a)-(d)  $\eta = 0.3$ , and (e)-(h)  $\eta = 0.1$



**Fig. 5** The quantitative analyses of the theoretical simulations with different anisotropic strength  $\eta$ : (a) the mean thickness, and (b) the surface roughness

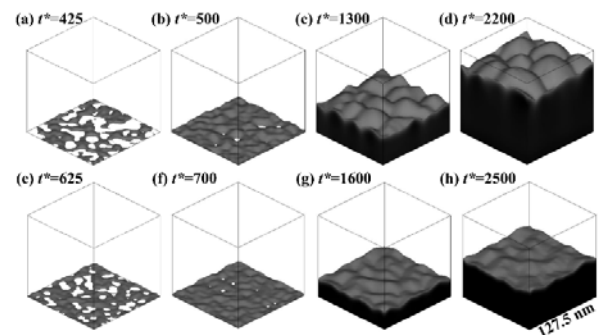
Since the adatoms would attach at certain crystallographic sites depending on the surface energies between the substrate, adatoms and solutions, the growth behavior of the film deposition is highly influenced by the solvent additives or the solution concentration in the chemical deposition. While the processing condition is altered, the growth model of the film deposition along a particular crystallographic direction would be changed. In this study, the preferred growth orientation of chemical deposition is further examined from  $\langle 100 \rangle$  into  $\langle 111 \rangle$  to theoretically exhibit the influence of preferred growth orientation on the surface formation. The surface morphological formation and profile evolution along  $\langle 111 \rangle$  preferred orientation during chemical deposition is presented in Fig. 6. In this case, the only difference in the simulation calculation is the preferred growth orientation in Eq. 7, while other parameters are the same used in Fig. 1. From Fig. 6, the processes of the nucleation and growth are distinctly revealed. Comparing Fig. 6 with Fig. 1, no obvious difference of the surface morphologies and evolutions could be seen in the  $\langle 100 \rangle$  preferred and  $\langle 111 \rangle$  preferred growth orientations. The surface feature in Fig. 6 has a pyramid-like morphology, which is similar to the surface characteristics in Fig. 1. The effect of the  $\langle 111 \rangle$  preferred orientation on the surface profile is obscure. It could be attributed to that the crystalline system of deposited films plays a dominant role by way of the atomic diffusion, not the growth orientation, during profile formation.



**Fig. 6** A theoretical simulation of chemical deposition process with  $\langle 111 \rangle$ -preferred growth orientation, calculated by Eq. (8)

The deposition rate of  $S_a^*$  are varied at different levels to analyze the preferred growth orientations for comparisons. Fig. 7(a)-(d) and (e)-(h) express the simulation results of chemical deposition with  $S_a^* = 0.1$  and  $0.05$  along  $\langle 111 \rangle$  preferred growth orientation, respectively. In the case of a high deposition rate, it could be seen that the nucleation of deposited films is boosted up, as shown in Fig. 7(a). Due to the high value of  $S_a^*$ , the growth rate of deposited film is also raised in the following deposition process, as demonstrated in

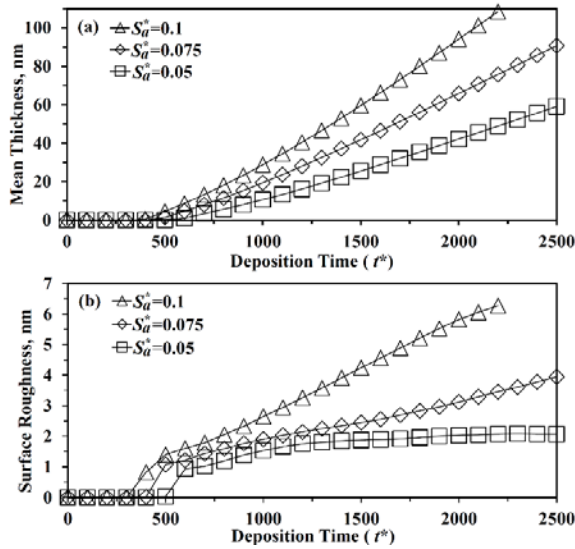
Fig. 7(b)-(d). In the initial stage of thin film formation, it is not easy to discover the difference of the morphological affected by the  $\langle 111 \rangle$  preferred growth orientation, as displayed in Fig. 7(a)-(b). While the deposition process is continued, the anisotropic growth gradually became a dominate role on the surface morphological formation owing to the high deposition rate. The characteristic profile of  $\langle 111 \rangle$  preferred growth orientation is transferred from a pyramid-like morphology to a bun-like profile with four-fold symmetry, as shown in Fig. 7(c)-(d). These simulation results also fit well with the experimental observations in Fig. 2 of Ref. Terasako et al. (2019). The morphological features are distinctly different to those with  $\langle 100 \rangle$  preferred growth orientation in Fig. 2(c)-(d). On the other hand, while the deposition rate of  $S_a^*$  is decreased to  $0.05$  with a  $\langle 111 \rangle$  preferred growth orientation, another type of surface morphology and evolution during chemical deposition is revealed. In Fig. 7(e)-(h) with a low deposition rate of  $S_a^*$ , it should be noticed that a slow process of the nucleation and growth of thin film formation is seen firstly based on the same time frame. In addition, since the low deposition rate is considered, the surface profile tends to be flattened during the evolution. Different to the case of a low deposition rate with a  $\langle 100 \rangle$  preferred growth orientation, a pyramid-like surface profile still could be distinguished in Fig. 2(e)-(f). However, in the condition of a low deposition rate with a  $\langle 111 \rangle$  preferred growth orientation, neither a pyramid-like morphology nor a four-fold symmetry surface profile is displayed. Instead, a mixture of multiple morphological profile with featureless surface is presented as shown in Fig. 7(g) and (h). It could be attributed to the conflict between the atomic diffusion and the preferred growth orientation. Under this condition, these two contradictory factors have a comparable influence on the surface morphological formation to cause this particular surface profile.



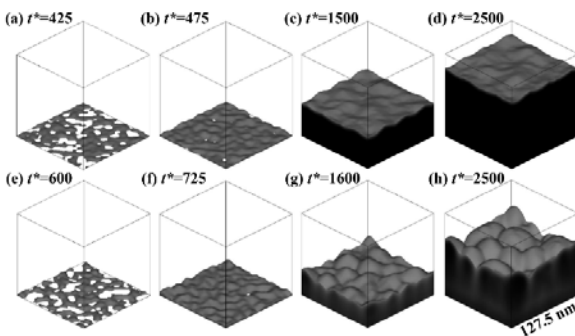
**Fig. 7** Theoretical simulations of chemical deposition process with different deposition rate  $S_a^*$  in a  $\langle 111 \rangle$ -preferred growth orientation condition, calculated by Eq. (8): (a)-(d) a high deposition rate of  $S_a^* = 0.1$ , and (e)-(h) a low deposition rate of  $S_a^* = 0.05$

Fig. 8 demonstrates the quantitative measurement of surface profiles for the various deposition rates

in  $\langle 111 \rangle$  preferred growth orientation. In Fig. 8(a), the influence of the deposition rate  $S_a^*$  on the mean film thickness during the deposition is presented, and a similar trend of the variations could be found in the condition of  $\langle 111 \rangle$  preferred growth orientation. As expected, the variation rate of deposited film thickness is proportional to the deposition rate  $S_a^*$ . Their slopes of the variation curves are 0.0267, 0.0402 and 0.0546 for  $S_a^* = 0.05, 0.075$  and  $0.15$ , respectively. In Fig. 8(b), the surface roughness is increased with the deposition rate  $S_a^*$ . While the surface roughness keeps at a low level for low deposition rate  $S_a^*$ , it increases with time and the deposition rate  $S_a^*$  in the high deposition rate  $S_a^*$ .



**Fig. 8** The quantitative analyses of the theoretical simulations with different deposition rate  $S_a^*$  in a  $\langle 111 \rangle$ -preferred growth orientation condition: (a) the mean thickness, and (b) the surface roughness



**Fig. 9** Theoretical simulations of chemical deposition process with different migration coefficient  $M_a^*$  in a  $\langle 111 \rangle$ -preferred growth orientation condition, calculated by Eq. (8): (a)-(d) a high migration coefficient of  $M_a^* = 0.02$ , and (e)-(h) a low migration coefficient of  $M_a^* = 0.005$

Finally, to discriminate the importance of atomic diffusion from the growth kinetics during chemical deposition, the parameter of migration coefficient  $M_a^*$

in Eq. 7 is varied with different values and the corresponding simulation results of morphological evolution and quantitative analyses are demonstrated in Fig. 9 and 10. Except the migration coefficient  $M_a^*$ , all other numerical parameters are comparable to the case of Fig. 6 to study the influence of migration coefficient during chemical deposition with  $\langle 111 \rangle$  preferred growth orientation. From Fig. 9(a) to (d), it could be found that in a high atomic migration coefficient the surface profile tends to be evolved into a flattened morphology. While a low atomic migration coefficient is considered, a characteristic surface morphology is revealed in the initial stage of film formation, as shown in Fig. 9(e) and (f). In the following stage, effected by  $\langle 111 \rangle$  preferred growth the crystallographic featured surface is strengthened and a four-fold column-like profile is evolved in Fig. 9(g) and (h). Under this situation, the impact of the anisotropic deposition kinetics is greater than the atomic diffusion on surface formation. Furthermore, the corresponding analyses of film thickness and surface roughness demonstrate the details of surface morphology in Fig. 10.

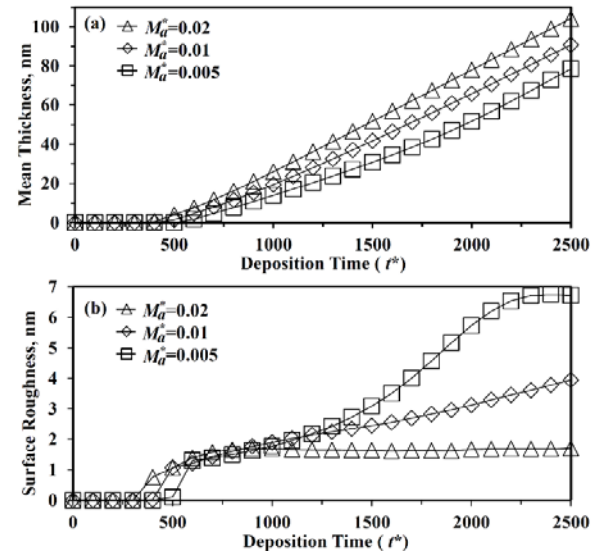


**Fig. 10** The quantitative analyses of the theoretical simulations with different migration coefficient  $M_a^*$  in a  $\langle 111 \rangle$ -preferred growth orientation condition: (a) the mean thickness, and (b) the surface roughness

Although the deposition rates  $S_a^*$  are identical in three conditions with different migration coefficient, the slopes of the film thickness with time are increased with the migration coefficient, as shown in Fig. 10(a). The slopes of the curves are 0.0463, 0.0402 and 0.0335 for  $M_a^* = 0.02, 0.01$  and  $0.005$ , respectively. From the point view of formation mechanism, the high migration coefficient would stimulate the adatoms to migrate to the energetically preferred sites. Subsequently, this situation might enhance the anisotropic growth along particular crystallographic orientation. As a low migration coefficient is considered, the anisotropic

growth with a less adatom migration would accumulate the adatoms along particular crystallographic orientation to cause a rougher surface. Thus, the surface roughness would be increased with a decreased migration coefficient. This consequence is clearly displayed in Fig. 10(b). These morphological simulations and quantitative measurements had distinctly demonstrated the influence of various deposition parameters on the surface formation and evolution during a chemical deposition. It provides many information and details to understand the mechanism of chemical deposition, which has a great benefit to facilitate the advanced manufacturing technology.

## CONCLUSIONS

In relative research of theoretical approaches, a phase field method is the most proper and efficient tools to inspect the precipitation problems. In this study, a numerical model of chemical deposition is built based on the theoretical mechanism to depict the formation and evolution of surface morphology during processing. Furthermore, individual parameters affecting the precipitation reactions are examined to theoretically demonstrate the influence on the surface morphologies and structures in a chemical deposition. The simulation calculations of the film evolution show the consistent results with the experimental observations. According to the numerical analysis, the pyramid-like surface morphologies are mainly attributed to the anisotropic surface diffusion and the surface roughness is in accord with the deposition rate. In addition, the roughness and the characteristic length of surface structures would increase with a high anisotropic strength. While a  $\langle 111 \rangle$  preferred growth orientation with a high deposition rate or a low migration coefficient is considered, the characteristic surface profile is transferred from a pyramid-like morphology to a bun-like profile with four-fold symmetry. All the factors of the deposition rate, atomic diffusion and anisotropic growth orientation could play the significant effects on the surface formation and evolution in a chemical deposition, depending on the various manufacturing conditions. With these systemic studies, the numerical results have provided the useful information for the chemical deposition to advance the design process of manufacturing parameters.

## ACKNOWLEDGMENT

This work is supported by Ministry of Science and Technology, Republic of China (Taiwan) under grant MOST 106-2221-E-024 -008 -MY3 and MOST 109-2221-E-024-007.

## REFERENCES

Arandhara, G., Bora, J. and Saikia, P.K., "Effect of pH on the crystallite size, elastic properties and

morphology of nanostructured ZnS thin films prepared by chemical bath deposition technique,"; *Mater. Chem. Phys.*, Vol. 241:122277(2020).

- Asp, K. and Ågren, J., "Phase-field simulation of sintering and related phenomena – a vacancy diffusion approach,"; *Acta Mater.*, Vol. 54, No. 5, pp. 1241-1248(2006).
- Cao ,M., Zhang, X., Ren, J., Sun, Y., Cui, Y., Zhang, J., Ling, J., Huang, J., Shen, Y., Wang, L. and Dai, N., "Chemical bath deposition of SnS: Cu/ZnS for solar hydrogen production and solar cells,"; *J. Alloys Compd.*, Vol. 863:158727(2021).
- Chen, L. and Yang, W., "Computer simulation of the domain dynamics of a quenched system with a large number of nonconserved order parameters: the grain-growth kinetics,"; *Phys. Rev. B*, Vol. 50:15752(1994).
- Chol, K.H., Ho, C.H., Jo, K.Y. and Il, S.G., "Effect of the reactant concentration, bath temperature and deposition time on the properties of CdS thin film prepared by the chemical bath,"; *Opt. Mater.*, Vol. 112:110790(2021).
- Dantzig, J.A., Napoli, P.D., Friedli, J. and Rappaz, M., "Dendritic growth morphologies in Al-Zn alloys – part II: phase-field computations,"; *Metall. Mater. Trans. A*, Vol. 44, pp. 5532-5543(2013).
- Duan, Z., Fu, X., Mei, Y., Hu, Z., Mao, J., Ding, K., You, C., Wang, X. and Zhao, G., "Annealing heating rate dependence of microstructure and multiferroic properties in Bi<sub>4</sub>Ti<sub>2.9</sub>Fe<sub>0.1</sub>O<sub>12</sub>/CoFe<sub>2</sub>O<sub>4</sub> layered magnetoelectric composite films prepared by chemical solution deposition method,"; *Ceram. Int.*, Vol. 46, No. 10, pp. 15654-15664(2020).
- Ghobadi, N., Chobin, S., Rezaee, S. and Shakoury, R., "Tuning the optical and photocatalytic features of copper selenide prepared by chemical solution deposition method,"; *Surf. Interfaces*, Vol. 21:100706(2020).
- Govender, K., Boyle, D.S., Kenway, P.B. and O'Brien, P., "Understanding the factors that govern the deposition and morphology of thin films of ZnO from aqueous solution,"; *J. Mater. Chem.*, Vol. 14, pp. 2575–2591(2004).
- Gu, P., Zhu, X. and Yang, D., "Vertically aligned ZnO Nanorods arrays grown by chemical bath deposition for ultraviolet photodetectors with high response performance,"; *J. Alloys Compd.*, Vol. 815:152346(2020).
- Gupta, I. and Mohanty, B.C., "Dynamics of surface evolution in semiconductor thin films grown from a chemical bath,"; *Sci. Rep.*, Vol. 6:33136(2016).
- Henry, H. and Levine, H., "Dynamic instabilities of fracture under biaxial strain using a phase field model,"; *Phys. Rev. Lett.*, Vol. 93:105504(2004).

- Hodes, G., *Chemical Solution Deposition of Semiconductor Films*, Marcel Dekker, New York, pp. 31-33(2002)
- Hone, F.G. and Dejene, F.B., Cationic concentration and pH effect on the structural, morphological and optical band gap of chemically synthesized lead sulfide thin films,”; *J. Mater. Res. Technol.*, Vol. 8, No. 1, pp. 467-474(2020).
- Jing, X.N., Zhao, J.H., Subhash, G. and Gao, X.-L., “Anisotropic grain growth with pore drag under applied loads,”; *Mater. Sci. Eng. A*, Vol. 412, pp. 271–278(2005).
- Kim, J., “Three-dimensional numerical simulations of a phase-field model for anisotropic interfacial energy,”; *Commun. Korean Math. Soc.*, Vol. 22, No. 3, pp. 453-464(2007).
- Kostoglou, M., Andritsos, N. and Karabelas, A.J., “Modeling thin film CdS development in a chemical bath deposition process,”; *Ind. Eng. Chem. Res.*, Vol. 39, No. 9, pp. 3272-3283(2000).
- Kostoglou, M., Andritsos, N. and Karabelas, A.J., “Incipient CdS thin film formation,”; *J. Colloid Interface Sci.*, Vol. 263, No. 1, pp. 177–189(2003).
- Li, K. and Dong, Y., “Modeling the influence of incident angle and deposition rate on a nanostructure grown by oblique angle deposition,”; *J. Phys. D: Appl. Phys.*, Vol. 50:065302(2017).
- Lipowsky, P., Hedin, N., Bill, J., Hoffmann, R.C., Ahniyaz, A., Aldinger, F. and Bergstrom, L., “Controlling the assembly of nanocrystalline ZnO films by a transient amorphous phase in solution,”; *J. Phys. Chem. C*, Vol. 112, pp. 5373-5383(2008).
- Lipowsky, P., Jia, S., Hoffmann, R.C., Phillip, N.Y.J., Bill, J. and Rühle, M., “Thin film formation by oriented attachment of polymer-capped nanocrystalline ZnO,”; *Int. J. Mater. Res.*, Vol. 97, No. 5, pp. 607-613(2006).
- McFadden, G.B., Wheeler, A.A., Braun, R.J., Coriell, S.R. and Sekerka, R.F., “Phase-field models for anisotropic interfaces,”; *Phys. Rev. E*, Vol. 48:2016(1993).
- Min, H. S., “Atomic force microscopy studies on the chemical bath deposited CuS films,”; *Orient. J. Chem.*, Vol. 32, No. 3, pp.1515-1519(2016).
- Mo, Y.W., Kleiner, J., Webb, M.B. and Lagally, M.G., “Activation energy for surface diffusion of Si on Si(001): a scanning-tunneling-microscopy study,”; *Phys. Rev. Lett.*, Vol. 66:1998(1991).
- Moelans, N., Blanpain, B. and Wollants, P., “An introduction to phase-field modeling of microstructure evolution,”; *Calphad: Comput. Coupling Ph. Diagr. Thermochem.*, Vol. 32, pp. 268–294(2008).
- Pauporte, T., “Preparation of ZnO Nanorods and Nanowires by Wet Chemistry,” in *Wide Band Gap Semiconductor Nanowires 1: Low-Dimensionality Effects and Growth*, ed. By V. Consonni and G. Feuillet, Wiley-ISTE, London, pp. 325(2014).
- Podmaniczky, F., Tóth, G.I., Pusztai, T. and Gránásy, L., “Free energy of the bcc-liquid interface and the Wulff shape as predicted by the phase-field crystal model,”; *J. Cryst. Growth*, Vol. 385, pp. 148-153(2014).
- Porter, D.A., Easterling, K.E. and Sherif, M.Y.A., *Phase Transformations in Metals and Alloys*, 3rd edn., CRC Press, Boca Raton, pp. 18-23(2009).
- Pourshaban, E., Abdizadeh, H. and Golobostanfard, M.R., “A close correlation between nucleation sites, growth and final properties of ZnO nanorod arrays: Sol-gel assisted chemical bath deposition process,”; *Ceram. Int.*, Vol. 42, No. 13, pp.14721-14729(2016).
- Qu, Y., Huang, X., Li, Y., Lin, G., Guo, B., Song, D. and Cheng, Q., “Chemical bath deposition produced ZnO nanorod arrays as an antireflective layer in the polycrystalline Si solar cells,”; *J. Alloys Compd.*, Vol. 698, pp.719-724(2017).
- Roa, S., Sandoval, M. and Sirena, M., “Chemical bath deposition of high structural and morphological quality PbSe thin films with potential optoelectronic properties for infrared detection applications,”; *Mater. Chem. Phys.*, Vol. 264:124479(2021).
- Schneller, T., Waser, R., Kosec, M. and Payne, D., *Chemical Solution Deposition of Functional Oxide Thin Films*, Springer-Verlag Wien, pp. 319-320(2013).
- Suo, Z. and Lu, W., “Forces that drive nanoscale self-assembly on solid surfaces,”; *J. Nanoparticle Res.*, Vol. 2, pp. 333-344(2000).
- Surabhi, S., Anurag, K., Rajpal, S. and Kumar, S.R., “A new route for preparing CdTe thin films by chemical bath deposition,”; *Mater. Today: Proc.*, Vol. 44, pp.1463-1467(2021).
- Terasako, T., Kitamoto, R. and Okada, H., “Fe-assisted chemical bath deposition of highly oriented Cu<sub>2</sub>O films and formation of ZnO nanorods/Cu<sub>2</sub>O heterojunctions,”; *Mater. Today: Proc.*, Vol. 7, pp. 784-791(2019).
- Tonagi, D., Hagiwara, M. and Fujihara, S., “Fabrication of highly (111)-oriented Cu<sub>2</sub>O films on glass substrates by repeated chemical bath deposition,”; *J. Cryst. Growth*, Vol. 551:125920(2020).
- Versteeg, H.K. and Malalasekera, W., *An Introduction to Computational Fluid Dynamics: The Finite Volume Method*, Longman Scientific &

- Technical, England, pp. 281-284(1995).
- Vinokur, M., "An analysis of finite-difference and finite-volume formulations of conservation laws,"; J. Comput. Phys., Vol. 81, No. 1, pp. 1-52(1989).
- Wang, Y.U., "Computer modeling and simulation of solid-state sintering: a phase field approach,"; Acta Mater., Vol. 54, No. 4, pp. 953-961(2006).
- Warren, J.A., Kobayashi, R., Lobkovsky, A.E. and Carter, W.C., "Extending phase field models of solidification to polycrystalline materials,"; Acta Mater., Vol. 51, No. 20, pp. 6035-6058(2003).
- Yahiro, J., Kawano, T. and Imai, H., "Nanometric morphological variation of zinc oxide crystals using organic molecules with carboxy and sulfonic groups,"; J. Colloid Interface Sci., Vol. 310, No. 1, pp. 302-311(2007).
- Younsi, A. and Cartalade, A., "On anisotropy function in crystal growth simulation using Lattice Boltzmann equation,"; J. Comput. Phys., Vol. 325, pp. 1-21(2016).
- Yu, H. and Lu, W., "Dynamics of the self-assembly of nanovoids and nanobubbles in solids,"; Acta Mater., Vol. 53, No. 6, pp. 1799-1807(2005).
- Zhang, C., Du, X. and Zhang, H., "Improved biaxial texture of tri-layer YBCO/CaTiO<sub>3</sub>/YBCO films using an all chemical solution deposition method,"; Phys. C: Supercond. Appl., Vol. 578:1353737(2020).

示薄膜金字塔形的表面形貌，透過優選生長方向的控制，可轉變為四重對稱的山脊狀表面形態。這些數值模擬展現了化學浴製程中薄膜沉積的成核和生長過程。本理論模型為化學浴沉積技術的發展提供了一有利的研究工具。

## 化學浴沉積之製程參數對表面形貌形成影響研究

李昆達 洪聖傑 胡漢霖 林大偉  
國立臺南大學材料科學系

### 摘要

化學浴沉積由於製程簡單與應用廣泛等特性，在許多現代化和先進製造領域中，扮演著重要的角色。在本研究中，採用了數值模擬方法來探討化學浴沉積之薄膜形成機制，重建薄膜沉積之表面形貌演化過程。在理論模型中，考慮了影響表面形貌的各種製程參數，透過數值計算模擬這些參數在化學浴沉積過程中對表面形貌形成與反應機制的影響。本研究的主要貢獻在於建立化學浴沉積製程之三維異向性數值模型，同時包含晶體異向性擴散與異向性成長。有系統地研究沉積速率、優選生長方向和擴散速率等製程因素，模擬出各種薄膜表面形貌的形成與演化。數值結果顯